# Single-cell dissection of urine-derived stem cell hierarchies reveals robust chondrogenesis and clinical scalability

Alexander Schulz[1], Emily Brockmann[1], Miriam Zentgraf[2], Andreas S. Baur[2], Steffen Uebe[1], Arif B. Ekici[1], Mark Dedden[3], Sebastian Zundler[3,4], Christian T. Thiel[1]

[1]Institute of Human Genetics, University Hospital Erlangen, FAU Erlangen-Nürnberg, Erlangen, Germany

[2]Department of Dermatology, University Hospital Erlangen, FAU Erlangen-Nürnberg, Erlangen, Germany

[3]Department of Medicine 1, University Hospital Erlangen and Friedrich-Alexander-University Erlangen-Nürnberg, Erlangen, Germany

[4]Deutsches Zentrum Immuntherapie (DZI), University Hospital Erlangen, Erlangen, Germany

## Abstract

Development of models of human cartilage and bone growth is essential for the study of growth disorders and pave the way for personalized therapeutic interventions. The majority of in vitro strategies depend on the use of invasively obtained mesenchymal stem cells (MSCs) or the generation of intricate induced pluripotent stem cells (iPSCs).We have established urine-derived stem cells (USCs) as a non-invasive stem cell source capable of osteogenic and robust chondrogenic differentiation in 3D. Single-cell RNA sequencing of USCs revealed a hierarchy originating from parietal epithelial cells of the kidney, with a proliferative *TOP2A*$^{+}$ subpopulation governed by *MYC* and *E2F4* regulatory networks. Integration of chondrogenic USCs with a human cartilage single-cell reference has led to the identification of a *TIMP3*$^{+}$-expressing chondrocyte-like subpopulation that exhibits cartilage-specific gene ontologies. Pseudotime analysis uncovers an *ALDH1A2*$^{+}$ intermediate state and alternative chondrogenic differentiation trajectories. In conclusion, a streamlined, xeno-free culture and differentiation protocol has been developed, thereby establishing a foundational framework for clinical-grade expansion and cartilage matrix formation. This positions USCs as a powerful model for cartilage biology and a platform for regenerative therapies.

**Keywords: skeletal dysplasia, cartilage, chondrocyte differentiation, urine-derived stem cells, xeno-free cell culture**

## Introduction

Developmental disorders of the skeleton have major implication for human health, but their underlying mechanisms remain only partly understood[1]. A notable manifestation is impaired longitudinal bone growth, which can manifest as short stature and affects up to 2.3% of the general population[2]. Growth disorders can be attributed to various etiologies, including genetic syndromes[3-6], endocrine defects[7-9], skeletal dysplasias[10,11], chronic diseases[12], and idiopathic short stature[13,14]. At the cellular level, the pathology may originate from any zone of the growth plate (reserve, proliferative, or hypertrophic) or from the metaphysis and epiphysis[15,16]. Disruption of the function of the cells that comprise the cartilage (chondrocytes) and the composition of the extracellular matrix (ECM) have been shown to impair the organization of growth plates, leading to abnormal bone elongation[15]. Genetic backgrounds encompass genes encoding growth plate matrix proteins, such as *COL2A1* mutations associated with spondyloepiphyseal dysplasia and hypochondrogenesis[17]; or *ACAN* mutations that result in premature growth plate closure[18]. Defects in the key regulators of cartilage cells such as Indian hedgehog, underlying brachydactyly type A1 and acrocapital femoral dysplasia[17] are also prominent. Within the aforementioned spectrum, skeletal dysplasias are of particular pertinence, with achondroplasia representing a prevalent form that affects more than 360,000 individuals worldwide[19].

However, research on disorders of cartilage and bone formation is restricted by the limited access to primary human chondrogenic tissue, as it is invasive and ethically constrained[20]. Consequently, the comprehension of skeletal disorders and the development of patient-specific therapies are frequently impeded by a paucity of suitable, accessible, and ethically acceptable cellular models. The majority of *in vitro* models used for studying chondrogenesis utilize either induced pluripotent stem cells (iPSCs) or mesenchymal stem cells (MSCs). MSCs, which possess the capacity to differentiate into cartilage, are obtained through an invasive procedure from tissue sources such as adipose tissue, bone marrow, and synovial fluid[21,22]. In contrast, iPSCs offer the benefit of a pluripotent and renewable source. However, these methods are expensive, time-consuming, and require substantial infrastructure for their derivation and differentiation, which limits their availability in typical or high-throughput research setups[23,24]. Moreover, their therapeutic value is further constrained by intrinsic tumorigenicity[25]. Consequently, both the MSC and iPSC approaches exhibit significant practical limitations when modeling and treating genetic skeletal diseases, particularly in cases that require repeated sampling or patient-specific studies.

Urine-derived stem cells (USCs) have emerged as a promising alternative to overcome these challenges[26]. These can be propagated economically without the need for surgical procedures[27]. Despite increasing interest in their cartilage regenerative capabilities[28-30], the application of USCs as a model system for cartilage and skeletal diseases has remained largely unexplored, particularly in the context of developmental skeletal disease modeling. In addition, the conventional culture of USCs, as initially identified in their original discovery[26], is intricate and reliant on animal-derived products. The utilization of this culture method is exclusively suitable in the context of in vitro research. This restriction is primarily attributed to the inherent risks associated with the transfer of animal factors to patients, the potential for immunological responses, and the presence of animal pathogens. These factors have the capacity to compromise the validity of study results and therapeutic interventions[31].

We hereby present USCs as a novel platform for investigating human chondrogenesis and modeling of genetic skeletal diseases. Furthermore, a simple, xeno-free culture and chondrogenic differentiation method for USCs is presented, which has the potential to pave the way for personalized, non-surgical medicine and cartilage regeneration.

## Results

### USCs are parietal epithelial cells derived from *MYC*- and *E2F4*- driven stem cells

Following the implementation of standard Seurat[32] QC procedures and the subsequent clustering of 19,024 cells, nine transcriptionally distinct clusters were identified (UMAP, Fig. 1A, B; QC details in Supplementary Fig. 1A–E). By scoring established urinary and renal gene sets (CellMarker 2.0[33]) in each cell, we confirmed the kidney origin of USCs (Fig. 1C). Anchor-based transfer from a published kidney atlas[34] successfully localized USCs to a parietal epithelial cell (PEC), late proximal tubule (LPT) or distal thin limb (DTL) identity (Fig. 1D, Supplementary Fig. 2A). Expression of PEC-specific markers was observed, and was most pronounced in Cluster 4, which also demonstrated highest mapping confidence (Fig. 1C–F).

However, given that many other clusters did not show a PEC marker gene expression signature, and USCs were previously reported to have multipotent differentiation capabilities[35], we investigated the drivers of stemness in these cells. The application of CytoTRACE2[36]-based stemness scoring revealed a negative correlation between clusters high in potency particularly the *TOP2A*$^+$ cluster in $G_2$/M phase, and PEC identity. VIPER inference further identified *E2F4* and *MYC* as master regulators of the stem-like state, whereas *KLF4* activity marked quiescent PEC-like clusters (Fig. 1G–I, Supplementary Fig. 2B).

### USCs possess osteogenic and robust chondrogenic differentiation potential

Given our interest in a cellular model for growth disorders, the subsequent step was to analyze and confirm the differentiation capabilities of USCs towards osteogenic and chondrogenic fate. CytoTRACE2 potency UMAP revealed that a considerable proportion of cells exhibited multipotency (Fig. 2A), thereby demonstrating the capacity to generate multiple cell types. Thus, USCs were cultured in differentiation media for 2 weeks, followed by staining of osteogenic-induced cells positive for calcium deposits. Chondrogenic cultures were positive for glycosaminoglycans (GAG) and formed chondrogenic aggregates, indicating cellular condensation observed during chondrogenic differentiation[37] (Fig. 2B).

Subsequently, we sought to ascertain whether these cells also express bona fide markers for osteoblast and chondrocytes. In order to screen multiple markers simultaneously, we performed bulk RNA sequencing. Bulk RNA-seq (PCA: Supplementary Fig. 2C) and reverse transcription quantitative polymerase chain reaction (RT-qPCR) validated successful lineage specification (Fig. 2C-F). Chondrogenic cultures exhibited a more pronounced upregulation of lineage-specific markers (Fig. 2D) in comparison to osteogenic cultures (Fig. 2C), (osteogenic: 2/4; chondrogenic 4/4 canonical markers), while both conditions increased late marker expression (osteogenic: *SPP1,* RQ undifferentiated = 0.149 ± 0.006; differentiated = 1.00 ± 0.0.06; n = 3; $p < 0.0001$; chondrogenic: *COL10A1*, RQ undifferentiated = 0.030 ± 0.013; differentiated = 1.00 ± 0.07; n = 3; $p < 0.01$), as confirmed by qPCR (Fig. 2E, F). Because monolayer chondrogenesis failed to induce *ACAN* (Fig. 2D), we transitioned to 3-week chondrospheres. These displayed strong aggrecan immunofluorescence only upon induction (Fig. 2G; Supplementary Video) and confirmed that USCs form bona fide cartilage matrix in 3D.

Taken together, our data demonstrates that USCs can differentiate along both osteogenic and especially chondrogenic pathways.

### Differentiation of USCs towards chondrogenic fate on single cell resolution

We confirmed the hypothesis that USCs are a unique PEC stem cell subpopulation (Fig. 1), with osteogenic and chondrogenic potential (Fig. 2), rather than conventional MSCs. Consequently, urine-

shed PECs may provide alternative differentiation pathways to MSCs. In accordance with the hypothesis that USC chondrogenesis might recapitulate the process of endochondral ossification, crucial for proper shape and growth of the skeleton[38], we sought to determine if the USCs lineage trajectory resembles differentiation towards functional chondrocytes.

The integration of 10,325 chondrogenic-stage cells (QC details in Supplementary Fig. 1F–J) with a healthy cartilage reference atlas demonstrated discrete separation from undifferentiated USCs (Concordance with bulk RNA-Seq Supplementary Fig. 2D, E) and mapped predominantly to reference cluster 4 (Supplementary Fig. 2E-K).

Pseudotime analysis (Slingshot[39]) delineated different trajectories from *TOP2A*$^+$ stem cells to chondrocyte-like clusters (Fig. 3 A, B, Supplementary Figure 2K), with late pseudo time nodes (*TIMP3*$^+$/*CDH1*$^+$/*LEF1*$^+$) enriched for autophagy and cellular respiration (Fig. 3C) and chondrocyte-differentiation GO terms in cluster 3 (Fig. 3F), with positive chondrocyte correlation (pearson R = 0.164 ± 0.092; n = 2753; Fig. 3A). RT-qPCR validated strong upregulation of *SOX9* (RQ undifferentiated = 0.017 ± 0.001; differentiated = 1.00 ± 0.23; n = 3; $p < 0.01$) and *TIMP3* (RQ undifferentiated = 0.011 ± 0.013; differentiated = 1.00 ± 0.91; n = 3; $p < 0.05$), (Fig. 3G, H), supporting the terminal chondrogenic identity of cluster 3. Additionally, analysis of gene expression confirmed that *SOX9*, *SOX5*, and *SOX6*, the core chondrogenic transcriptional trio[40], were predominantly expressed in late chondrogenic clusters (Cluster 2, 3, 7, 8, 10; Fig. 3B, D, E, Supplementary Fig. 2E), reinforcing their role in USCs cartilage lineage commitment and further validating the chondrogenic identity of terminal states.

**USCs are suitable for clinical applications**

We optimized a xeno-free workflow by substituting FBS with autologous human serum (HS) and adding fibroblast growth factor 2 (FGF2; Supplementary Fig. 3A, B). Full HS-expanded USCs (HS-USC) exhibited a modest decrease in proliferation compared to cells expanded in FBS (Supplementary Fig. 3C), higher *KLF4* (PEC-like; RQ FBS = 1.00 ± 0.06; RQ HS = 1.80 ± 0.39; n = 3; $p < 0.05$) and higher *MYC* (Stem cell-like; RQ FBS = 1.00 ± 0.11; RQ HS = 1.25 ± 0.12; n = 3; $p < 0.05$) expression (Fig. 4A, B).

The chondrogenic potential of HS versus FBS expanded cells were assessed, either in presence of HS (chHS), or FBS (chFBS). Cells cultivated and differentiated in HS displayed strong cellular condensation upon chondrogenic induction, in contrast to those in FBS conditions (Fig. 4C). GAG accumulation was found to be significantly higher in FBS controls (OD650/DNA in FBS = 0.01 ± 0.0003, OD650/DNA in HS = 0.006 ± 0.0004, n = 4; $p < 0.0001$), (Fig. 4D).

As the results obtained suggested enhanced differentiation in 3D (Fig. 2G), we additionally performed chondrogenic differentiation in pellets. *TOP2A* marker expression (proliferative cells) remained stable upon induction in HS-USC (RQ undifferentiated = 1.37 ± 0.08; RQ differentiated = 1.46 ± 0.53, n = 3), but strongly downregulated in FBS conditions (RQ undifferentiated = 3.28 ± 0.72; RQ differentiated = 0.54 ± 0.08, n = 3, $p < 0.001$), (Fig. 4E).

Chondrogenic pellets from HS-USCs expressed *SOX9* more strongly (RQ chFBS = 0.61 ± 0.02; RQ chHS = 1.39 ± 0.07; n = 3; $p < 0.0001$), hinting towards clinically feasible and chondrogenic potential (Fig. 4F). Additionally, expression of the later pseudo time genes (Fig. 3B, C) *TIMP3* (RQ chFBS = 0.19 ± 0.04; RQ chHS = 1.81 ± 0.36; n = 3; $p < 0.001$) and *CDH1* (RQ chFBS = 0.18 ± 0.03; RQ chHS = 1.81 ± 0.25; n = 3; $p < 0.001$) was strongly increased in chondrogenic HS pellet culture conditions (Fig. 4G, H), confirming stronger lineage specification in HS.

## Discussion

We demonstrate that urine-shed parietal epithelial cells (USCs) present a transcriptionally distinct, *MYC*/*E2F4*-driven progenitor population with robust chondrogenic potential and clinical scalability. In contrast to classical bone marrow-derived MSCs[21,22], USCs are derived non-invasively from human urine, expand efficiently in xeno-free conditions, and differentiate into cartilage-like tissues with in 3D environments. These characteristics position USCs as a uniquely accessible and translationally relevant stem cell source. The noninvasive nature of USCs facilitates repeated treatment or monitoring of the same patient, impossible with bone-marrow MSCs or biopsies.

Single-cell RNA sequencing confirmed that USCs are a stem-like subpopulation of renal parietal epithelial cells rather than conventional MSCs. The transcriptional landscape of these cells is governed by a regulatory axis comprising *MYC*/*E2F4*, with heightened activity observed in proliferative subsets (Fig. 1I, H). While the oncogenic potential of *MYC*'s is well established[41], its role in this context may reflect physiological re-entry from quiescence rather than neoplastic transformation[42]. Despite the elevated *KLF4* expression exhibited by USCs from our HS protocol for clinical translation (Fig. 4A, PEC identity), and their apparent genetic stability[26], further evaluation is necessary to ascertain the long-term genomic stability and tumorigenicity of these cells under regenerative protocols.

USCs exhibit both osteogenic and chondrogenic differentiation potential; however, transcriptomic analysis reveals a pronounced propensity toward chondrogenesis (Fig. 2 C/D). Although expression of osteogenic markers and calcium deposition can be detected, chondrogenic marker (ACAN) expression—particularly within three-dimensional culture systems such as spheres or pellets—is substantially elevated (Fig. 2). This bias may be influenced by the formation of 3D cellular condensates that mimic mesenchymal condensation during chondrogenesis[37]. Consequently, it is concluded that chondrogenic USCs should be cultured in either spheres or pellets for a 3D implementation.

The application of pseudo time modeling revealed the existence of disparate principal differentiation trajectories (Fig. 3B). One of these populations resulted in a *SOX9*$^{+}$/*TIMP3*$^{+}$ population (Cluster 3; Fig. 3B–E) that exhibited similarity to healthy articular chondrocytes (Fig. 3A) and enrichment for chondrogenic differentiation pathways (Fig. 3F). As indicated by the increased expression of both genes in HS-USC (Fig. 4F, G), there is a probable enhancement of the differentiation process related to cartilage formation in xeno-free conditions. A second terminal *CDH1*$^{+}$ cluster co-expressing SOX transcription factors (Cluster 10; Fig. 3C–E) may mark progenitors competent for the aforementioned mesenchymal condensation[37,43]. As greater condensation was also observed in HS-USC (Fig. 4C), increased *CDH1* expression was confirmed (Fig. 4H), in alignment with robust condensate building competency.

Taken together, chondrogenic USCs in chondrogenic FBS conditions are stimulated to produce ECM rich in GAGs (Fig. 4D). However, HS has been shown to stimulate chondroprogenitor condensation and thereby mimicking the process of embryonic cartilage development[44], which is reflected by increased expression of *CDH1* and the terminal state pseudo time marker, *TIMP3*. This assertion is further substantiated by the observation that HS-USC exhibits elevated levels of stemness-related *MYC* expression (Fig. 4B). Depending on the desired outcome of USCs chondrogenesis, either GAG-rich ECM synthesis, or resembling embryonic cartilage development, can be taken into consideration.

Subsequent observations revealed that *TOP2A* expression remained consistent in the presence of HS conditions, a finding that was indicative of proliferative stem cell cluster cells (Fig. 1B, G, H, 3C), in contrast to FBS where expression drops (4E). This phenomenon can be explained by a tissue homeostasis mechanism driven by HS, possibly resembling progenitors also seen in cartilage in order to respond to injury[45]. Subsequent research endeavors should prioritize the elucidation of the

identity of these cells, as this could facilitate the determination of final differentiation to be dictated by the in vivo environment following transplantation.

It is noteworthy that chondrogenic branches originated from undifferentiated *ALDH1A2*$^+$ progenitors enriched for the GO-term "chondrocyte differentiation", suggesting that retinoic acid related[46] metabolic pre-patterning plays a role in lineage bias (Cluster 0; Fig. 3C, D, F; Supplementary Fig. 2E). This finding suggests the potential for a strategy to modify the fate decisions of USCs, or to enrich for proliferative (*MYC*$^+$/*E2F4*$^+$) or chondrogenic (*ALDH1A2*$^+$) subpopulations. This transcriptional distinctness and lineage bias broaden the known spectrum of renal-derived stem cells, with implications for engineering specialized musculoskeletal tissues.

The findings of our study position USCs as a tractable model for studying cartilage development, disease modeling, and regenerative repair. In contrast to the invasive procurement methods employed in the context of MSCs, USCs offer a scalable, non-invasive, and potentially GMP-compatible alternative (Fig. 4). This characteristic aligns with the clinical demands for autologous and xeno-free cell therapies. This observation is further substantiated by the doubling time during the exponential growth phase of our study, (HS: 31.9 hours, FBS: 29.8 hours), which is intermediate between the doubling times of neonatal (~ 24 h) and adult tissue (~ 40 h) derived MSCs[47,48]. The xeno-free HS + FGF2 workflow was utilized to achieve an expanded state with chondrogenic stem cells as early as 20 days, with costs of approximately $100 per donor (Supplementary Table 1). This approach demonstrates a marked economic advantage compared to induced pluripotent stem cells (iPSCs), which typically require over $10,000 for generation and validation [49].

In conclusion, our findings position urine-derived stem cells (USCs) as a uniquely accessible and clinically viable cell source for cartilage research and regenerative therapies. Through an integrated approach that combines single-cell transcriptomics, functional assays, three-dimensional differentiation models, and a xeno-free expansion protocol, we delineate the molecular and cellular landscape underpinning the robust chondrogenic potential of USCs. This comprehensive framework not only elucidates the mechanisms driving their lineage commitment but also sets the stage for translational studies in skeletal regeneration and disease modeling. Collectively, these data provide a blueprint for leveraging USCs in clinically relevant, autologous, and scalable applications for cartilage tissue engineering and regenerative medicine.

## Methods

### Urine stem cell isolation and culture

Urine was centrifuged at 300 g. cell pellet was washed with PBS 1% Penicillin Streptomycin (Gibco) and pelleted cells cultured after repeated centrifugation. Culture medium consisted of a 1:1 mixture of DMEM high glucose (Gibco), containing 1 % NEAA (Gibco) and 1 % Penicilin Streptomycin (Gibco), with KSFM (Gibco), with addition of 15 % FBS (Sigma Aldrich or Roth) and 5 ng/mL FGF2 (Peprotech) or humankine thermostable FGF2 (Sigma). For an animal free workflow, we harvested USCs in the same manner, this time resupending the cellular pellet in either Alpha MEM Eagle medium (PAN Biotech) supplemented 5 ng/mL FGF2 (Sino Biological) with 10% FBS (Sigma-Aldrich or Roth) as the FBS-Control, or in 10 % autologous human serum. All cell lines generated for this study were from the same donor, and no passages greater 5 were used. Culture medium was exchanged three times per week.

### Proliferation curves

To compare proliferation, we seeded FBS- and HS-derived USCs of the same passages in triplicates onto 96 well plates at a density of 1000 cells per well, and counted cells manually with trypan blue

exclusion every second day. Doubling time was calculated for cells in the exponential growth phase (day 4-8) as the following:

$$Growth\ rate\ k = \frac{\Delta(\ln N)}{\Delta t}$$

$$Doubling\ time\ DT = \frac{\ln 2}{k}$$

**Urine stem cell differentiation and staining**

Chondrogenic differentiation was induced with the StemPro Chondrogenesis Kit (Gibco). Osteogenic induction was facilitated with an osteogenic medium described by zhang et al [50]. Differentiation lasted for two weeks with media change three times per week. Wells with cells for bulk RNA-Seq were coated with 0.2 % gelatin solution. To stain glycosaminoglycans in chondrogenic, and calcium deposits in osteogenic cells, we fixed cells with 4 % paraformaldehyde, washed with PBS, and stained for one hour with 1 % Alcian Blue 8GX (Sigma) in 3 % acidic acid or Alizarin Red Solution (Merck Millipore). After a final washing step with PBS images were taken under a VertA1 (Zeiss) microscope. A separate USC line, harvested at a different time point from the same donor, was cultured for 2 days in Alpha MEM Eagle medium (PAN Biotech) supplemented with 10% fetal bovine serum (FBS; Sigma-Aldrich or Roth) and 5 ng/mL FGF2 (Sino Biological), and served as the non-induced control.

For a comparative pellet culture between HS- or FBS-USCs, we centrifuged 250000 USCs at 300 g for 10 min in 15 ml falcon tubes (Corning) and incubated with in house made chondrogenic media. The media recipe was: DMEM HG with pyruvate (Gibco), human recombinant insulin 6.25 µg/mL (Merck), human holo-transferrin 6.25 µg/mL (Sigma Aldrich), sodium selenite 6.7 ng/mL (Sigma Aldrich), 10 % Serum (autologous human serum or FBS, Roth) 10 ng/mL recombinant human TGF-Beta 1 (Peprotech), 100 ng/mL recombinant human IGF1, 100 nm Dexmethason (Sigma Aldrich), 50 µg/mL ascorbate-6-phosphate (Sigma Aldrich).

Alcian blue quantification was performed by lysing cells for 2 hours at room temperature with 6M Guanidine hydrochloride (Sigma). Absorbance was measured at 650 nm. For normalization to DNA content, DNA was extracted from control wells with the DNeasy Blood & Tissue Kit (Qiagen).

**Single-cell RNA sequencing and data Processing**

USCs and chondrogenic USCs were subjected to single-cell RNA sequencing (scRNA-seq) to characterize transcriptomic profiles in undifferentiated and chondrogenically differentiated states. Cell fixation, barcoding, cDNA amplification and Libraries were prepared using Parse Biosciences Parse Evercode WT V3 Workflow and sequenced on Illumina NovaSeq X Plus. FASTQ files were processed using Trailmaker™ pipeline module (https://app.trailmaker.parsebiosciences.com/; pipeline v1.5.0, Parse Biosciences). Raw count matrices and associated metadata were processed in Seurat (version 5.3.0)[32] in R. Cells with <1st or >99th percentile of gene counts or Unique Molacular Identifier (UMI) counts, or >95th percentile mitochondrial reads, were excluded. Data were normalized (LogNormalize), variable features (n = 2,000) identified (vst), and counts scaled while regressing out nCount_RNA and percent.mt. PCA (dims 1–20) was followed by UMAP visualization and Louvain clustering (resolution = 0.5). Cluster markers were identified via Wilcoxon testing (min.pct = 0.25). For visualization of data we used Seurat´s DotPlot, VlnPlot or DimPlots and the R packages ggplot2 (version 3.5.2)[51], ggrepel (version 0.9.6)[52], viridis (version 0.6.5)[53] and RColorBrewer (version 1.1.3)[54].

**Tissue origin and cell-type annotation**

Marker lists for human urinary and renal tissues were curated from CellMarker 2.0[33], filtered for uniqueness across tissues, and scored per cell using Seurat's AddModuleScore. Complementary AUC enrichment was computed with AUCell (version 1.30.1)[55] on the normalized data. To assign putative cell identities, we leveraged a well-annotated human kidney atlas (Tisch et al.[34]) as a reference. Briefly, the atlas and our USC Seurat object were first normalized and dimensionally reduced in parallel. We then computed integration anchors between the reference and query using FindTransferAnchors. Cell-type labels stored in the reference metadata were projected onto the query via TransferData. Finally, we summarized mapping confidence by computing the median prediction.score.max within each Seurat cluster to guide downstream cluster ordering and interpretation.

**Stemness inference and transcription-factor activity mapping**

CytoTRACE2 (version 1.1.0)[36] was run on the top 10,000 variable genes (counts slot) to assign each cell a continuous stemness score. Cells were binned into five quantile-defined stemness groups. We inferred per-cell transcription-factor activities using VIPER (version 1.42.0)[56] with high-confidence DoRothEA (version 1.20.0)[57] A/B regulons on the Seurat-normalized data slot. TF activities were merged into the metadata alongside CytoTRACE2 scores and UMAP coordinates. For each stemness group (the five quintile bins), we computed the mean activity of every TF and selected the top three TFs uniquely highest in each group. To visualize regulatory dynamics, we computed Spearman correlations between TF activities and CytoTRACE2 scores across all cells, identifying the top 20 TFs most strongly associated with stemness.

**Cell cycle analysis**

Cell cycle phase assignment was performed using the built-in Seurat gene sets for S phase and G2/M phase genes. The Seurat function CellCycleScoring was applied to the processed data, utilizing the predefined sets of cell cycle genes for the S and G2/M phases. Each cell was classified into one of the four phases: G1, S, G2/M, or unassigned. Phase information was then merged with cluster identities, and the proportion of cells in each cell cycle phase per cluster was calculated.

**Bulk RNA-sequencing**

RNA was extracted from USC samples with RNeasy Mini Kit (Qiagen)with DNAse digestion, according to manufacturer. A cDNA library was generated for each sample using the Illumina stranded mRNA kit. Paired-end sequencing of the libraries with a fragment length of 159bp was conducted on an Illumina NovaSeq6000 platform. Raw data was then converted into reads and demultiplexed using Illumina Dragen Software (v. 3.8.4).

Unwanted RNA was filtered from the reads using bwa mem (version 0.7.17-r1188, arXiv:1303.3997) in combination with samtools (version 1.17[58]) and converted back into fastq format using the SamToFastq tool from GATK (version 4.2.1.0[59]). Reads from each sequencing lane were aligned individually to the hg38 reference genome with Ensembl (release 110[60]) gene annotations using STAR (version 2.7.10a[61]). For each sample, resulting alignments were combined using the MergeSamFiles command from Picard (version 2.25.4, http://broadinstitute.github.io/picard/). Gene quantification in form of a count matrix was generated using featureCounts (version 2.0.1[62]) and Ensembl gene annotations corresponding to those of the alignment reference. Alignment and quantification levels were used for quality assessment.

**Differential gene expression analysis**

Raw gene-level count data were obtained from bulk RNA-sequencing of three undifferentiated and three differentiated (osteogenic or chondrogenic) USC samples. Differential gene expression (DGE)

analysis was conducted using the DESeq2 package (version 1.48.1)[63] in R (version 4.5). For each comparison, gene-level counts were used to construct a DESeqDataSet object, with group labels assigned as the experimental condition. The DESeq2 pipeline was run with default parameters using DESeq(), and differential expression results were extracted using the results() function, specifying contrasts such that log2 fold changes represented upregulation in the differentiated condition relative to WT. Genes with an adjusted p-value (Benjamini-Hochberg method) less than 0.05 were considered statistically significant. Gene annotations were retrieved by mapping Ensembl IDs to HGNC symbols using the org.Hs.eg.db package (version 3.21.0)[64]. Differential expression results were visualized using volcano plots created with the ggplot2[51] and ggrepel[52] packages. Sample metadata was generated to define the experimental condition associated with each sample (WT, chWT, oWT), and this metadata was used to create a DESeqDataSet object using the DESeq2 package. The dataset was then log-transformed using the regularized log (rlog) transformation to stabilize variance across the dynamic range of expression levels. To improve PCA interpretability and reduce noise, features (genes) with negligible or zero variance were removed. Columns (genes) with variance less than 1e-6 or equal to zero were filtered out. Rows (samples) with zero variance across retained genes were also removed. PCA was performed on the transposed, filtered, and normalized gene expression matrix using the base R prcomp() function with centering and scaling enabled. The first three principal components were extracted for visualization. The resulting PCA scores were visualized using the plotly package (version 4.11.0)[65] to generate an interactive 3D scatter plot. The final plot was exported as an HTML widget using the htmlwidgets package (version 1.6.4)[66].

**Reverse transcriptase quantitative PCR**

RNA was extracted from USC samples with RNeasy Mini Kit (Qiagen) with DNAse digestion, according to manufacturer. Alternatively, we used NucleoSpin RNA Plus (Machery Nagel) with gRNA removal column. We made sure to use samples prepared with the same procdures for comperative anlysis. For cDNA Synthesis LunaScript RT SuperMix Kit (New Englang Biolabs) was used. RT-qPCR was performed with TaqMan Master-Mix and predesigned Assays (Applied Biosystems) on the Quantstudio 12K Flex Platform (Applied Biosystems). *RPLP0* served as housekeeping gene. RQ values were calculated with the delta delta CT (ddCT) method and four technical replicates. Statistics (unpaired welch´s t-test of ddCT values) and visualization were performed in R studio and Graphpad Prism (version 10). We always used three biological replicates per condition.

**3D-culture and immunofluorescence**

20000 USCs were seeded in each well of a 96 well Nunclon Sphera ultra low attachment cell culture plate (ThermoFisher Scientific) and centrifuged for 10 minutes at 300 g to enable scaffold free cellular self-aggregation. Cells were cultured for 3 weeks with StemPro Chondrogenesis Kit (Gibco). As an undifferentiated control we used USCs from the same donor (different batch), which were cultured 2 days in Alpha MEM Eagle (PAN Biotech) with 10 % FBS (Sigma Aldrich or Roth) and 5 ng/mL FGF2 (SinoBiological).

For immunofluorescent staining, spheres were fixed for one hour with 4 % paraformaldehyde (PFA) at room temperature. In the following, the spheroids were permeabilized with Triton X-100 for 30 minutes and then blocked with 1 % bovine serum albumin (Sigma-Aldrich) in PBS for 45 minutes. For primary antibody incubation anti-aggrecan (ab3778, abcam) was used in a concentration of 1:500 for one hour, followed by one hour of secondary anti-mouse antibody (AlexaFluor 488, Invitrogen) in a 1:500 dilution, with DAPI (1:1000, thermo fisher scientific). After washing with PBS spheroids were mounted with aqua polymount (Polysciences) on concave slides (Paul Marienfeld). Pictures were taken with the Axio Imager 2 with Apotome (Zeiss) and 25 Z-stacks. We used the same exposure times for differentiated and undifferentiated spheroids (DAPI: 10 ms, Aggrecan: 35 ms). The same

image enhancements for each condition, including normalization to DAPI and 3D animation, were performed with FIJI[67].

**Merging undifferentiated and chondrogenic USC datasets**

Undifferentiated and chondrogenic USC Seurat objects were annotated with a stage metadata field ("undiff" vs. "chondrogenic"). The two objects were merged and reprocessed end-to-end (NormalizeData, FindVariableFeatures, ScaleData, RunPCA, RunUMAP, FindNeighbors, FindClusters) to generate a unified embedding for downstream trajectory and mapping analyses. Results comparing chondrogenic and undifferentiated samples were obtained from DESeq2 analysis (adjusted p-value < 0.01, log2 fold change > 1). For proving concordance with bulk RNA-Sequencing, we extracted significantly upregulated genes and calculated a gene module score in the merged Seurat object. The AddModuleScore function was applied to quantify the expression of this gene set across cells. Resulting module scores were visualized on a UMAP embedding using the FeaturePlot function.

**Construction of healthy cartilage reference atlas and label transfer onto merged USC dataset**

We assembled a multi-sample single-cell reference from publicly available human cartilage data[68]. For each of the three selected samples, raw count matrices, feature, and barcode files were imported into Seurat. Cells with < 200 genes, < 3 cells per gene, or > 10% mitochondrial reads were excluded. Each sample was SCTransformed (regressing out percent.mt), then merged into a single Seurat object. We first applied the same QC filters as for our USC objects to the published cartilage reference to generate a high-quality "healthy cartilage" atlas. Cells annotated as normal cartilage were subsetted, and all assay layers were collapsed into a single RNA assay. This object was then log-normalized (NormalizeData), variable features were identified (FindVariableFeatures), data were scaled (ScaleData), and PCA (dims 1–30), neighbor-graph construction, clustering, and UMAP were performed. The merged undifferentiated + chondrogenic USC object underwent the same SCT-assay preprocessing. We then selected the top 3,000 integration features across both objects and computed label-transfer anchors with FindTransferAnchors (normalization.method = "SCT"). Finally, reference cluster identities were projected onto the USC dataset via TransferData, yielding per-cell predicted cluster labels and confidence scores, which were appended to the USC metadata.

**Mapping and correlation of USCs to chondrogenic reference atlas and pseudotime inference**

We loaded the processed human cartilage reference and the mapped USC dataset into Seurat (SCTransform normalization). To identify "cluster 4–like" USCs, we labeled any cell whose transferred reference cluster equaled "4" and whose PredictionScore > 0.7. Next, we computed the mean SCT embedding for reference cluster 4 and, for each USC cell, calculated the Pearson correlation between its SCT profile and the cluster 4 embedding. These correlation coefficients were then overlaid on the merged UMAP embedding to show how closely individual USCs resemble cluster 4 in principal component space. For pseudotime analysis, we ran Slingshot (version 2.16.0)[39] on the UMAP data, using the mitotic (*TOP2A*$^{+}$) cluster as the root. Slingshot automatically detected terminal states and lineages. We computed pseudotime values per cell, appended them to the USC metadata, and projected them onto the UMAP. Finally, we annotated clusters based on their top marker genes (FindAllMarkers) and performed Gene Ontology biological process enrichment (clusterProfiler, version 4.16.0)[69]. We mapped DE genes to Entrez IDs, ran enrichGO with Benjamini–Hochberg correction, and selected the top ten GO–BP terms per cluster. These process annotations, and their positions on the UMAP, were summarized and visualized using cluster centroids.

**Chondrogenic cluster annotation and functional characterization**

To identify clusters with chondrogenic potential, we integrated transcriptomic similarity to a reference chondrocyte population, GO enrichment, and expression of canonical marker genes. Average "cluster 4–like" scores (Pearson correlation to reference cluster 4) were computed per cluster and visualized with VlnPlot. The Z-score normalized, scaled average expression of chondrogenic markers (*SOX9*, *SOX5*, *SOX6*) were calculated and depicted in a heatmap. GO biological process enrichment was filtered to include only terms related to chondrocyte differentiation (GO:0032330, GO:0002062), and enrichment values were visualized with ggplot2 across clusters.

## Data availability

All sequencing data generated in this study have been deposited in the Gene Expression Omnibus (GEO) database. scRNA-Seq of USCs: accession code GSE307232. Bulk-RNA-Seq of USCs: accession code GSE306729. RT-qPCR raw and analyzed tables, differential gene expression tables of bulk RNA-Seq confirming differentiation, Top 10 and chondrocyte related GO-Terms per cluster, as well as marker genes for clusters used in chondrogenic trajectory analysis are in Supplementary Data.

## Code availability

All the R codes used to generate the results of this study will be publicly available on GitHub: https://github.com/alexschulzcell/USC-paper.

## References


1. Formosa, M.M. *et al.* A Roadmap to Gene Discoveries and Novel Therapies in Monogenic Low and High Bone Mass Disorders. *Front Endocrinol (Lausanne)* **12**, 709711 (2021).
2. Sharma, L., Rani, D., Kanchan, T. & et al. Short Stature. in *StatPearls [Internet]* (StatPearls Publishing, Treasure Island (FL), 2025).
3. Butler, M.G. Prader-Willi syndrome: current understanding of cause and diagnosis. *Am J Med Genet* **35**, 319-32 (1990).
4. Clement-Jones, M. *et al.* The short stature homeobox gene SHOX is involved in skeletal abnormalities in Turner syndrome. *Human Molecular Genetics* **9**, 695-702 (2000).
5. Noonan, J.A. Noonan syndrome and related disorders: alterations in growth and puberty. *Rev Endocr Metab Disord* **7**, 251-5 (2006).
6. Price, S.M., Stanhope, R., Garrett, C., Preece, M.A. & Trembath, R.C. The spectrum of Silver-Russell syndrome: a clinical and molecular genetic study and new diagnostic criteria. *J Med Genet* **36**, 837-42 (1999).
7. Lindsay, R., Feldkamp, M., Harris, D., Robertson, J. & Rallison, M. Utah Growth Study: Growth standards and the prevalence of growth hormone deficiency. *The Journal of Pediatrics* **125**, 29-35 (1994).
8. Kotake, M. *et al.* Short stature due to growth hormone deficiency associated with Cushing's disease and ulcerative colitis. *Horm Metab Res* **28**, 565-9 (1996).
9. Al-Omari, A.F. & Omer, Z.K. The impact of juvenile hypothyroidism on stature. *J Med Life* **16**, 1211-1214 (2023).
10. Seema, Abbas, S., Ahsan, M.N. & Asghar, M.S. Frequency of skeletal dysplasia in children with short stature presenting to endocrine clinic: An observational study. *J Family Med Prim Care* **11**, 3143-3147 (2022).
11. Sentchordi-Montané, L. *et al.* High prevalence of variants in skeletal dysplasia associated genes in individuals with short stature and minor skeletal anomalies. *Eur J Endocrinol* **185**, 691-705 (2021).
12. Kyle, U.G., Shekerdemian, L.S. & Coss-Bu, J.A. Growth failure and nutrition considerations in chronic childhood wasting diseases. *Nutr Clin Pract* **30**, 227-38 (2015).
13. Ranke, M.B. Towards a Consensus on the Definition of Idiopathic Short Stature. *Hormone Research* **45**, 64-66 (2008).

14. Wit, J.M. *et al.* Idiopathic short stature: definition, epidemiology, and diagnostic evaluation. *Growth Horm IGF Res* **18**, 89-110 (2008).
15. Argente, J., Tatton-Brown, K., Lehwalder, D. & Pfäffle, R. Genetics of Growth Disorders—Which Patients Require Genetic Testing? *Frontiers in Endocrinology* **Volume 10 - 2019**(2019).
16. Voller, T., Cameron, P., Watson, J. & Phadnis, J. The growth plate: anatomy and disorders. *Orthopaedics and Trauma* **34**, 135-140 (2020).
17. Phornphutkul, C. & Gruppuso, P.A. Disorders of the growth plate. *Current Opinion in Endocrinology, Diabetes and Obesity* **16**(2009).
18. Nilsson, O. *et al.* Short Stature, Accelerated Bone Maturation, and Early Growth Cessation Due to Heterozygous Aggrecan Mutations. *The Journal of Clinical Endocrinology & Metabolism* **99**, E1510-E1518 (2014).
19. Foreman, P.K. *et al.* Birth prevalence of achondroplasia: A systematic literature review and meta-analysis. *American Journal of Medical Genetics Part A* **182**, 2297-2316 (2020).
20. Phull, A.R., Eo, S.H., Abbas, Q., Ahmed, M. & Kim, S.J. Applications of Chondrocyte-Based Cartilage Engineering: An Overview. *Biomed Res Int* **2016**, 1879837 (2016).
21. Neybecker, P. *et al.* Respective stemness and chondrogenic potential of mesenchymal stem cells isolated from human bone marrow, synovial membrane, and synovial fluid. *Stem Cell Res Ther* **11**, 316 (2020).
22. Kangari, P., Talaei-Khozani, T., Razeghian-Jahromi, I. & Razmkhah, M. Mesenchymal stem cells: amazing remedies for bone and cartilage defects. *Stem Cell Res Ther* **11**, 492 (2020).
23. Moy, A.B., Kamath, A., Ternes, S. & Kamath, J. The Challenges to Advancing Induced Pluripotent Stem Cell-Dependent Cell Replacement Therapy. *Med Res Arch* **11**(2023).
24. Doss, M.X. & Sachinidis, A. Current Challenges of iPSC-Based Disease Modeling and Therapeutic Implications. *Cells* **8**(2019).
25. Lee, A.S., Tang, C., Rao, M.S., Weissman, I.L. & Wu, J.C. Tumorigenicity as a clinical hurdle for pluripotent stem cell therapies. *Nat Med* **19**, 998-1004 (2013).
26. Zhang, Y. *et al.* Urine derived cells are a potential source for urological tissue reconstruction. *J Urol* **180**, 2226-33 (2008).
27. Zhang, D., Wei, G., Li, P., Zhou, X. & Zhang, Y. Urine-derived stem cells: A novel and versatile progenitor source for cell-based therapy and regenerative medicine. *Genes Dis* **1**, 8-17 (2014).
28. Wan, S. *et al.* Extracellular Vesicles from Hypoxic Pretreated Urine-Derived Stem Cells Enhance the Proliferation and Migration of Chondrocytes by Delivering miR-26a-5p. *Cartilage* **13**, 19476035221077401 (2022).
29. Sun, J. *et al.* Comparison of chondrogenesis-related biological behaviors between human urine-derived stem cells and human bone marrow mesenchymal stem cells from the same individual. *Stem Cell Research & Therapy* **12**, 366 (2021).
30. Pei, M. *et al.* Matrix from urine stem cells boosts tissue-specific stem cell mediated functional cartilage reconstruction. *Bioactive Materials* **23**, 353-367 (2023).
31. Bui, H.T.H., Nguyen, L.T. & Than, U.T.T. Influences of Xeno-Free Media on Mesenchymal Stem Cell Expansion for Clinical Application. *Tissue Eng Regen Med* **18**, 15-23 (2021).
32. Hao, Y. *et al.* Dictionary learning for integrative, multimodal and scalable single-cell analysis. *Nature Biotechnology* **42**, 293-304 (2024).
33. Hu, C. *et al.* CellMarker 2.0: an updated database of manually curated cell markers in human/mouse and web tools based on scRNA-seq data. *Nucleic Acids Research* **51**, D870-D876 (2022).
34. Tisch, A. *et al.* Identification of kidney cell types in scRNA-seq and snRNA-seq data using machine learning algorithms. *Heliyon* **10**(2024).
35. Bharadwaj, S. *et al.* Multipotential differentiation of human urine-derived stem cells: Potential for therapeutic applications in urology. *Stem Cells* **31**, 1840-1856 (2013).
36. Kang, M. *et al.* Mapping single-cell developmental potential in health and disease with interpretable deep learning. *bioRxiv*, 2024.03.19.585637 (2024).

37. Tacchetti, C. *et al.* Cell condensation in chondrogenic differentiation. *Experimental Cell Research* **200**, 26-33 (1992).
38. Alman, B.A. Skeletal dysplasias and the growth plate. *Clinical Genetics* **73**, 24-30 (2008).
39. Street, K. *et al.* Slingshot: cell lineage and pseudotime inference for single-cell transcriptomics. *BMC Genomics* **19**, 477 (2018).
40. Lefebvre, V. Roles and regulation of SOX transcription factors in skeletogenesis. *Curr Top Dev Biol* **133**, 171-193 (2019).
41. Dhanasekaran, R. *et al.* The MYC oncogene - the grand orchestrator of cancer growth and immune evasion. *Nat Rev Clin Oncol* **19**, 23-36 (2022).
42. Jha, R.K., Kouzine, F. & Levens, D. MYC function and regulation in physiological perspective. *Front Cell Dev Biol* **11**, 1268275 (2023).
43. Marie, P.J. *et al.* Cadherin-mediated cell-cell adhesion and signaling in the skeleton. *Calcif Tissue Int* **94**, 46-54 (2014).
44. Fowler, D.A. & Larsson, H.C.E. The tissues and regulatory pattern of limb chondrogenesis. *Developmental Biology* **463**, 124-134 (2020).
45. Jiang, Y. & Tuan, R.S. Origin and function of cartilage stem/progenitor cells in osteoarthritis. *Nat Rev Rheumatol* **11**, 206-12 (2015).
46. Zhu, L. *et al.* Variants in ALDH1A2 reveal an anti-inflammatory role for retinoic acid and a new class of disease-modifying drugs in osteoarthritis. *Science Translational Medicine* **14**, eabm4054.
47. Hass, R., Kasper, C., Böhm, S. & Jacobs, R. Different populations and sources of human mesenchymal stem cells (MSC): A comparison of adult and neonatal tissue-derived MSC. *Cell Communication and Signaling* **9**, 12 (2011).
48. Petrenko, Y. *et al.* A Comparative Analysis of Multipotent Mesenchymal Stromal Cells derived from Different Sources, with a Focus on Neuroregenerative Potential. *Scientific Reports* **10**, 4290 (2020).
49. Huang, C.-Y. *et al.* Human iPSC banking: barriers and opportunities. *Journal of Biomedical Science* **26**, 87 (2019).
50. Zhang, C. *et al.* Reno-protection of Urine-derived Stem Cells in A Chronic Kidney Disease Rat Model Induced by Renal Ischemia and Nephrotoxicity. *International Journal of Biological Sciences* **16**, 435-446 (2020).
51. Valero-Mora, P.M. ggplot2: Elegant Graphics for Data Analysis. *Journal of Statistical Software, Book Reviews* **35**, 1 - 3 (2010).
52. Slowikowski, K. ggrepel: Automatically Position Non-Overlapping Text Labels with 'ggplot2'. (2024).
53. Garnier, S. *et al.* sjmgarnier/viridis: CRAN release v0.6.3 (v0.6.3CRAN). (Zenodo, 2023).
54. Neuwirth, E. RColorBrewer: ColorBrewer Palettes. 1.1-3 edn (R package, 2022).
55. Aibar, S. *et al.* SCENIC: single-cell regulatory network inference and clustering. *Nature Methods* **14**, 1083-1086 (2017).
56. Alvarez, M.J. *et al.* Functional characterization of somatic mutations in cancer using network-based inference of protein activity. *Nat Genet* **48**, 838-47 (2016).
57. Garcia-Alonso, L., Holland, C.H., Ibrahim, M.M., Turei, D. & Saez-Rodriguez, J. Benchmark and integration of resources for the estimation of human transcription factor activities. *Genome Res* **29**, 1363-1375 (2019).
58. Danecek, P. *et al.* Twelve years of SAMtools and BCFtools. *Gigascience* **10**(2021).
59. McKenna, A. *et al.* The Genome Analysis Toolkit: a MapReduce framework for analyzing next-generation DNA sequencing data. *Genome Res* **20**, 1297-303 (2010).
60. Dyer, S.C. *et al.* Ensembl 2025. *Nucleic Acids Res* **53**, D948-d957 (2025).
61. Dobin, A. *et al.* STAR: ultrafast universal RNA-seq aligner. *Bioinformatics* **29**, 15-21 (2013).
62. Liao, Y., Smyth, G.K. & Shi, W. featureCounts: an efficient general purpose program for assigning sequence reads to genomic features. *Bioinformatics* **30**, 923-30 (2014).
63. Love, M.I., Huber, W. & Anders, S. Moderated estimation of fold change and dispersion for RNA-seq data with DESeq2. *Genome Biology* **15**, 550 (2014).

64. Carlson, M. org.Hs.eg.db: Genome wide annotation for Human. (2024).
65. Sievert, C. Interactive Web-Based Data Visualization with R, plotly, and shiny. (2020).
66. Vaidyanathan, R. *et al.* htmlwidgets: HTML Widgets for R. **1.6.4**(2023).
67. Schindelin, J. *et al.* Fiji: an open-source platform for biological-image analysis. *Nature Methods* **9**, 676-682 (2012).
68. Huang, C. *et al.* Single-cell transcriptomic analysis of chondrocytes in cartilage and pathogenesis of osteoarthritis. *Genes & Diseases* **12**, 101241 (2025).
69. Yu, G., Wang, L.-G., Han, Y. & He, Q.-Y. clusterProfiler: an R Package for Comparing Biological Themes Among Gene Clusters. *OMICS: A Journal of Integrative Biology* **16**, 284-287 (2012).

## Figure Legends

**Figure 1: Transcriptional identity and stemness architecture of USCs.** A: Uniform Manifold Approximation and Projection (UMAP) of USCs with biological top markers annotated per cluster. B: Dotplot of biological top marker expression across cluster. C: AUC-based enrichment scores of bladder and kidney-specific expression profiles projected onto UMAP space. D: UMAP of predicted cell types from label transfer of kidney reference cell types. (Cells of ascending loop of Henle = ALH, of the parietal epithelium = PECs, of late proximal tubule = LPT, of distal thin limb = DTL, of proximal tubule = PT). E: Dotplot showcasing expression of PEC markers among clusters. F: The mapping of the confidence of individual clusters to the PECs/LPT/DTL of reference is a critical step in the analysis. G: CytoTRACE2 scoring of individual clusters. H: Cell cycle phase proportions of individual clusters. I: Top 3 TFs per stemness group overlaid onto CytoTRACE2 score (Score) based UMAP in a percentage-based color gradient manner. (darker boxes = more stemness and vice versa.)

**Figure 2: Functional differentiation capacity of USCs.** A: CytoTRACE2 potency UMAP depicting differentiation capacities across cells. B: GAC and calcium staining of uninduced (negative) or induced (positive) cells. (osteo= osteogenic differentiation stained with alcian blue, chondro= chondrogenic differentiation stained with alizarin red). C/D: Volcanoplots of osteogenic/chondrogenic differentiation, with labelled marker genes (genes highlighted: adjusted p-values < 0.05, log2 fold change > ± 1). E: SPP1 expression levels in undifferentiated (USC) and osteogenic (oUSC) cells as measured by RT-qPCR. F: RQ values of COL10A1 of USCs (USC) and chondrogenic (chUSC) cells. Bar with undetermined CT-values or exceeding 40 cycles, was marked (=ND). G= Immunofluorescence staining of uninduced (negative), or chondrogenically induced spheroids (sphere 1-3). (Scale bar represents 200 µm). (**, **** = p-value < 0.01, 0.0001.)

**Figure 3: Single-cell lineage trajectories toward chondrocyte-like states.** A: Violinplot highlighting correlation to chondrocyte reference cluster across merged undifferentiated and chondrogenic USC object clusters. B: UMAP of merged USC object with slingshot pseudotime gradient and chondrogenic lineage curves. C: UMAP of the merged USC object with top marker annotation, chondrogenic lineage curves and summary of biological process GO-terms. D: UMAP of the merged USC object with cluster number annotation E: Heatmap, depicting the z-score normalized expression of SOX- transcription factors among clusters. F: Dotplot depicting clusters, enriched for chondrocyte related GO-terms. G/H: SOX9 and TIMP3 expression levels in undifferentiated and chondrogenic cells as measured by RT-qPCR in chondrogenic cells and undifferentiated controls. Bar with undetermined CT-values or exceeding 40 cycles, was highlighted (=ND). (*, ** = p-value < 0.05, 0.01)

**Figure 4: Xeno-free (HS) expansion enhances clinically relevant chondrogenesis.** A/B: KLF4/MYC expression levels in FBS-USC (FBS) and HS-USC (HS) cells as measured by RT-qPCR C: Alcian blue quantification of chondrogenic FBS-USC (chFBS) or chondrogenic HS-USC (chHS). D: Alcian blue staining of chFBS or chHS. E/F/G/H: RQ values of different markers of uninduced USCs (USC) and chondrogenic (chUSC) cells in pellet culture, comparing FBS or HS culture conditions. Bar with undetermined CT-values or exceeding 40 cycles, was marked (=ND). (*, **, ***, **** = p-value < 0.05, 0.01, 0.001, 0.0001).


## Acknowledgments

We thank Mohammad Deen Hayatu and Evelyn Galsterer for technical assistance. This work was funded by the Deutsche Forschungsgemeinschaft (DFG, German Research Foundation) – [TH896 7-1].


## Author information

### Contributions

A.S: performed the experiments, processed and analyzed all data, and wrote the original draft, E.B: processed the raw bulk RNA sequencing data. M.Z: revised figures, manuscript and contributed to xenofree media development, A.S.B: revised manuscript, S.U: guidance in bioinformatics, A.B.E: assisted with sample collection, M.D: processed raw single cell RNA sequencing data, S.Z: revised manuscript, A.R: revised manuscript, C.T.T: project P.I, acquired funding, supervised research and study design, and revised manuscript

## Ethics declarations

### Competing interests

The authors declare no competing interests.

Fig. 1

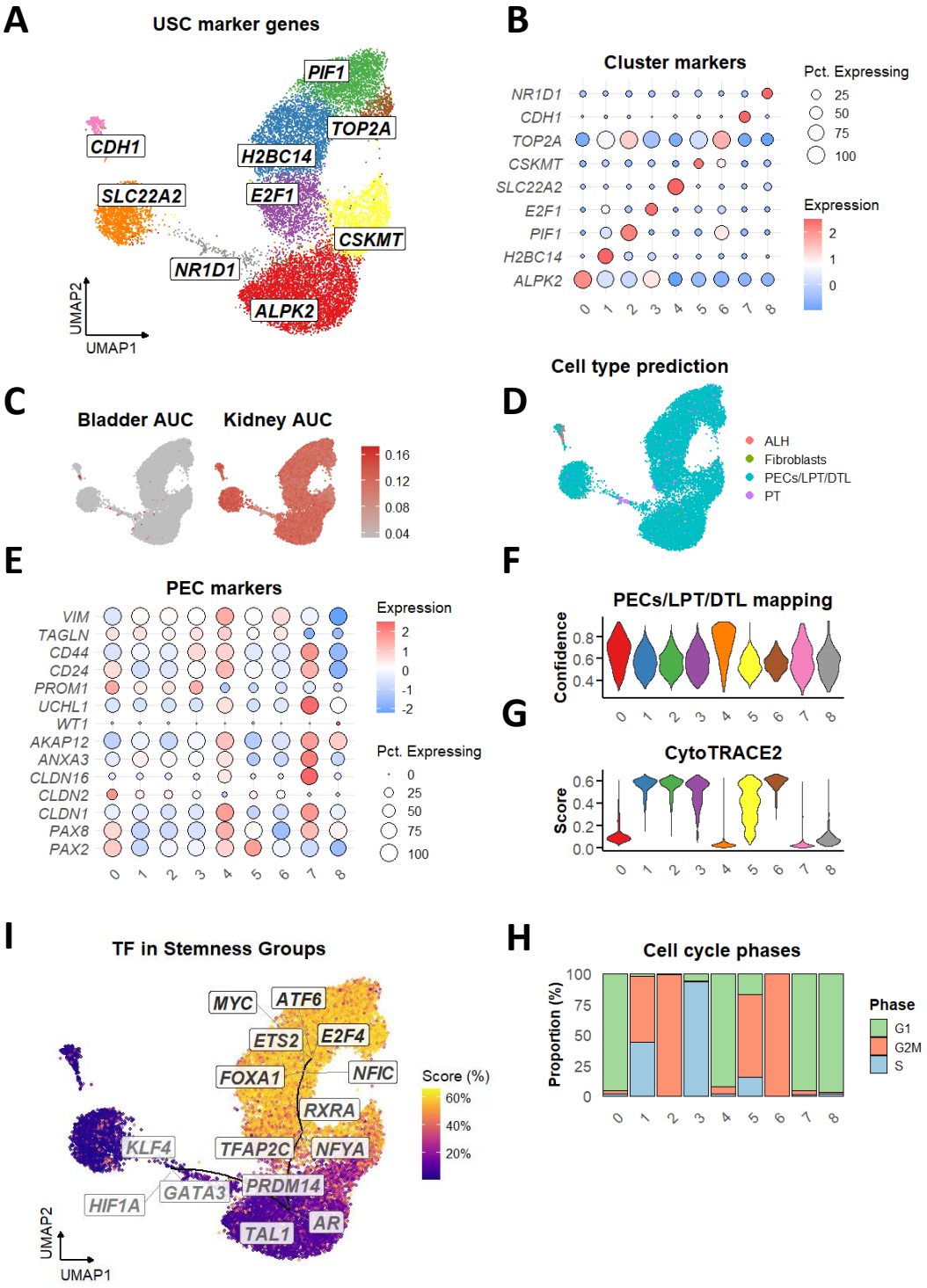
A
USC marker genes
PIF1
TOP2A
CDH1
H2BC14
SLC22A2
E2F1
CSKMT
NR1D1
ALPK2
UMAP2
UMAP1
B
Cluster markers
NR1D1
CDH1
TOP2A
CSKMT
SLC22A2
E2F1
PIF1
H2BC14
ALPK2
0 1 2 3 4 5 6 7 8
Pct. Expressing
25
50
75
100
Expression
2
1
0
C
Bladder AUC
Kidney AUC
0.16
0.12
0.08
0.04
D
Cell type prediction
ALH
Fibroblasts
PECs/LPT/DTL
PT
E
PEC markers
VIM
TAGLN
CD44
CD24
PROM1
UCHL1
WT1
AKAP12
ANXA3
CLDN16
CLDN2
CLDN1
PAX8
PAX2
Expression
2
1
0
-1
-2
Pct. Expressing
0
25
50
75
100
F
PECs/LPT/DTL mapping
Confidence
0.8
0.6
0.4
G
CytoTRACE2
Score
0.6
0.4
0.2
0.0
I
TF in Stemness Groups
MYC
ATF6
ETS2
E2F4
FOXA1
NFIC
RXRA
KLF4
TFAP2C
NFYA
HIF1A
GATA3
PRDM14
TAL1
AR
Score (%)
60%
40%
20%
UMAP2
UMAP1
H
Cell cycle phases
Proportion (%)
100
75
50
25
0
Phase
G1
G2M
S

Fig. 2

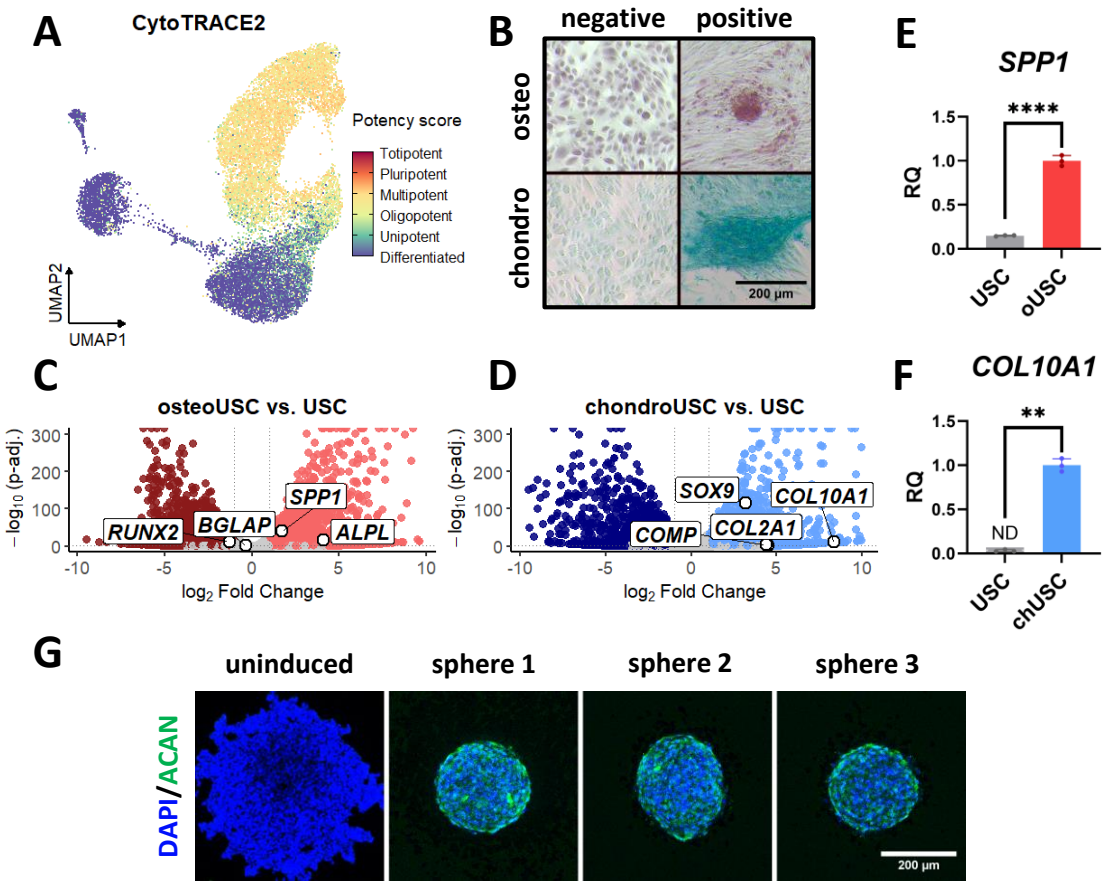
A
CytoTRACE2
Potency score
Totipotent
Pluripotent
Multipotent
Oligopotent
Unipotent
Differentiated
UMAP2
UMAP1
B
negative
positive
osteo
chondro
200 µm
E
SPP1
****
RQ
1.5
1.0
0.5
0.0
USC
oUSC
C
osteoUSC vs. USC
−log10 (p-adj.)
300
200
100
0
RUNX2
BGLAP
SPP1
ALPL
-10
-5
0
5
10
log2 Fold Change
D
chondroUSC vs. USC
SOX9
COL10A1
COMP
COL2A1
F
COL10A1
**
ND
USC
chUSC
G
uninduced
sphere 1
sphere 2
sphere 3
DAPI/ACAN
200 µm

Fig. 3

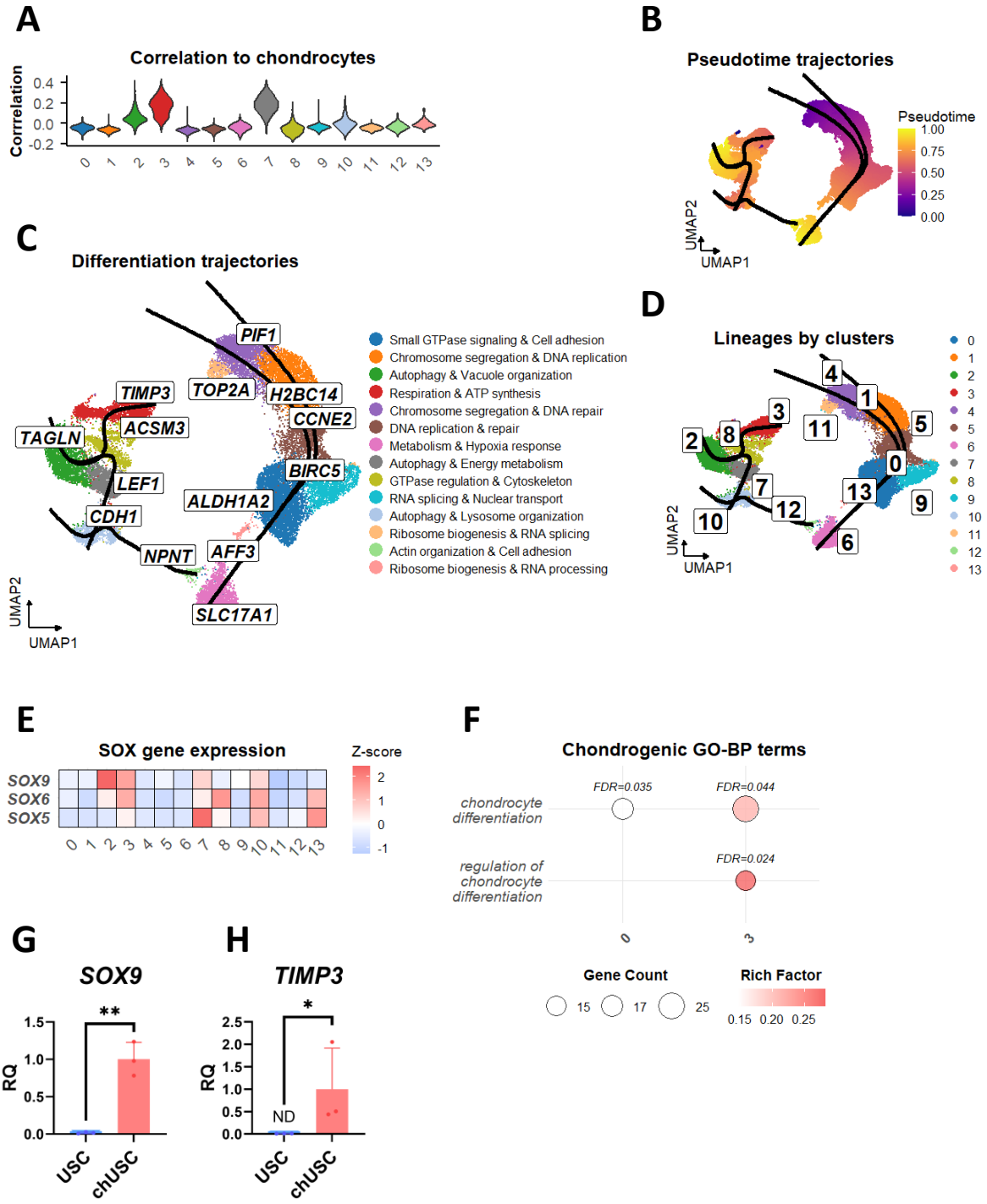
A
Correlation to chondrocytes
Corrrelation
0.4
0.2
0.0
-0.2
0 1 2 3 4 5 6 7 8 9 10 11 12 13
B
Pseudotime trajectories
Pseudotime
1.00
0.75
0.50
0.25
0.00
UMAP2
UMAP1
C
Differentiation trajectories
PIF1
TOP2A
H2BC14
CCNE2
TIMP3
ACSM3
TAGLN
LEF1
BIRC5
ALDH1A2
CDH1
NPNT
AFF3
SLC17A1
UMAP2
UMAP1
Small GTPase signaling & Cell adhesion
Chromosome segregation & DNA replication
Autophagy & Vacuole organization
Respiration & ATP synthesis
Chromosome segregation & DNA repair
DNA replication & repair
Metabolism & Hypoxia response
Autophagy & Energy metabolism
GTPase regulation & Cytoskeleton
RNA splicing & Nuclear transport
Autophagy & Lysosome organization
Ribosome biogenesis & RNA splicing
Actin organization & Cell adhesion
Ribosome biogenesis & RNA processing
D
Lineages by clusters
4
1
3
11
5
2
8
0
7
13
9
12
10
6
UMAP2
UMAP1
0 1 2 3 4 5 6 7 8 9 10 11 12 13
E
SOX gene expression
Z-score
SOX9
SOX6
SOX5
2
1
0
-1
0 1 2 3 4 5 6 7 8 9 10 11 12 13
F
Chondrogenic GO-BP terms
FDR=0.035
FDR=0.044
chondrocyte differentiation
FDR=0.024
regulation of chondrocyte differentiation
0
3
Gene Count
15 17 25
Rich Factor
0.15 0.20 0.25
G
SOX9
**
RQ
1.5
1.0
0.5
0.0
USC
chUSC
H
TIMP3
*
RQ
2.5
2.0
1.5
1.0
0.5
0.0
ND
USC
chUSC

Fig. 4

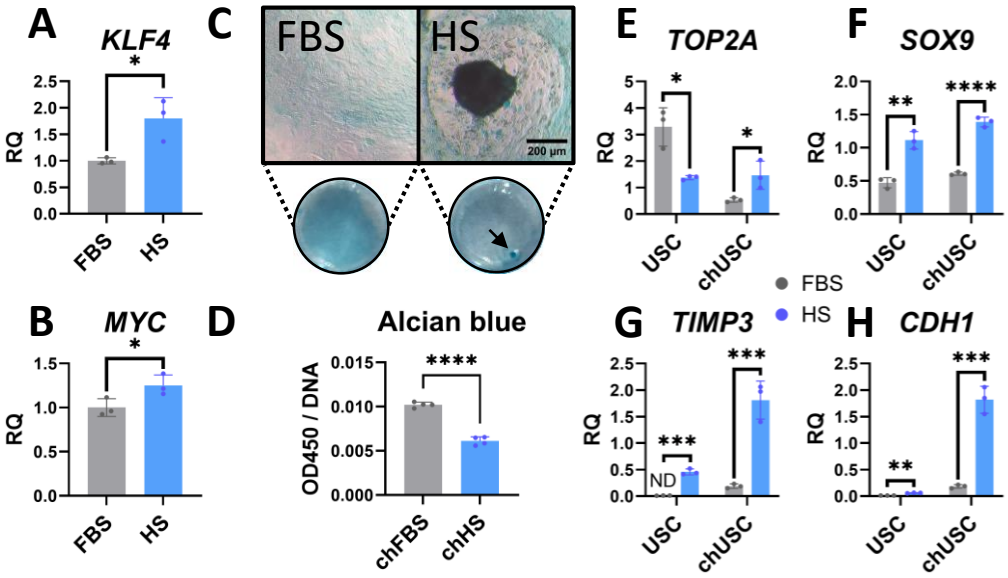
A
KLF4
RQ
FBS
HS
B
MYC
C
FBS
HS
200 µm
D
Alcian blue
OD450 / DNA
chFBS
chHS
E
TOP2A
F
SOX9
USC
chUSC
FBS
HS
G
TIMP3
ND
H
CDH1